

Optimization of reactively sputtered Mn_3GaN films based on resistivity measurements

Christoph Sürgers^{1,*}, Gerda Fischer¹, Sihao Deng^{2,3}, Dongmei Hu⁴, and Cong Wang^{4,5}

¹*Karlsruhe Institute of Technology, Physikalisches Institut, P.O. Box 6980, D-76049 Karlsruhe, Germany*

²*Institute of High Energy Physics, Chinese Academy of Sciences, Beijing 100049, China*

³*Spallation Neutron Source Science Center, Dongguan 523803, China*

⁴*School of Physics, Beihang University, Beijing 100191, China and*

⁵*School of Integrated Circuit Science and Engineering, Beihang University, Beijing 100191, China*

(Dated: May 3, 2024)

Mn-based nitrides with antiperovskite structures have several properties that can be utilised for antiferromagnetic spintronics. Their magnetic properties depend on the structural quality, composition and doping of the cubic antiperovskite structure. Such nitride thin films are usually produced by reactive physical vapour deposition, where the deposition rate of N can only be controlled by the N_2 gas flow. We show that the tuning of the N content can be optimised using low temperature resistivity measurements, which serve as an indicator of the degree of structural disorder. Several Mn_3GaN_x films were prepared by reactive magnetron sputtering under different N_2 gas flows. Under optimised conditions, we obtain films that exhibit a metal-like temperature dependence, a vanishing logarithmic increase in resistivity towards zero, the highest resistivity ratio and a lattice contraction of 0.4 % along the growth direction when heated above that of the Néel temperature in agreement with the bulk samples.

I. INTRODUCTION

Intermetallic compounds with antiperovskite structures provide several interesting physical and chemical properties that can be exploited for technical purposes such as advanced batteries, magnetoresistance, adjustable thermal expansion behavior, and luminescence [1, 2]. In particular, Mn-based antiperovskites Mn_3AX ($\text{A} = \text{Co}, \text{Ni}, \text{Zn}, \text{Ga}, \text{Ge}, \text{Ag}, \text{Zn}; \text{X} = \text{N}, \text{C}$) are multifunctional materials with strong magnetostructural and magnetoelastic coupling that give rise to considerable magnetovolume effects, piezomagnetism, enhanced barocaloric response, and giant magnetostriction [1, 3–7]. In Mn_3AX , the Mn atoms in the (111) planes of the cubic structure are arranged in a kagome lattice with antiferromagnetically coupled magnetic moments. The geometrical frustration between the moments leads to coplanar but noncollinear Γ^{4g} or Γ^{4g} magnetic structures with very low magnetization [2, 8–10]. The noncollinear antiferromagnetic order is the origin of important magnetic properties like the anomalous Hall effect (AHE), spin Hall effect, and spin torque switching that can be utilized in future antiferromagnetic spintronic devices [11–13]. The magnetic configuration strongly affects the AHE, where Γ^{4g} and Γ^{5g} have a finite or zero AHE, respectively [14]. These magnetic antiperovskites are often susceptible to biaxial strain and tetragonal distortions which can lead to the appearance or enhancement of a AHE [15].

However, small variations in stoichiometry can lead to substantial changes of the structural and magnetic properties [16–19]. N deficiency often leads to an increase of the Néel temperature T_N and a broadening of the phase transition observed in the thermal expansion [16, 20]. Usually, structural analysis by X-ray or neutron

diffraction is used for tuning and optimizing the alloy composition to obtain the structural or magnetic properties. Recently, detailed structural analysis demonstrated that the displacement of Mn atoms lowers the symmetry of the system, thereby allowing the generation of a nonzero AHE, which would otherwise cancel out in a perfect crystal by spin rotation of different antiferromagnetic domains [21].

While much work has been done on bulk compounds obtained by solid-state reactions at high temperatures, the synthesis of films with reasonable structural order is challenging, particularly when performed in a reactive environment as necessary for the preparation of nitride films. In this respect, electrical resistance is a physical property that is easy to measure, albeit often difficult to interpret, and sensitive to the effects of disorder and structural and magnetic phase transitions. It provides a method to optimize the deposition conditions to obtain the desired film composition. In this work we have investigated Mn_3GaN_x films obtained by reactive magnetron sputtering on MgO substrates in Ar atmosphere under different N_2 flows Φ . Mn_3GaN is a noncollinear antiferromagnet with T_N between 280 and 380 K [10, 17, 20, 22]. $T_N = 300$ K observed for bulk Mn_3GaN is shifted to 380 K by strain in $\text{Mn}_3\text{GaN}/\text{Pt}$ bilayers [23] and electrical current switching of the magnetization has been demonstrated [22]. By analyzing the temperature dependence of the resistivity $\rho(T)$ at low temperatures, we obtain optimized sputtering conditions for synthesis of thin films with minimized structural disorder.

II. EXPERIMENTAL

Substrates were cleaned and heated to 500 °C in a vacuum chamber with a base pressure in the low 10^{-6} mbar range. Films were deposited by dc magnetron sputtering

* christoph.suergers@kit.edu

from a single $\text{Mn}_{75}\text{Ga}_{25}$ alloy target.

Reactive magnetron sputtering is a complex process where the reactive gas reacts at the target, the substrate surface, and at the chamber walls. The stoichiometric and physical properties of the film substantially depend on the type of the reactive gas, the gas flow, and deposition power. The gas flow affects the compound formation of the film due to different deposition modes, i.e., compound formation on the substrate (metal mode) or on the target (poisoned mode), non-linear dependencies of the deposition rate on the flow rate, etc. [24, 25]. Due to the number of parameters that influence film growth and compound formation, films reported in this study were deposited always at a total pressure of 10^{-2} mbar, constant dc power of 81 W, constant flow of 40 sccm Ar but with different N_2 gas flows $\Phi = 0 - 5$ sccm. Typical growth rates were 0.03 nm/s. Some films were patterned for resistivity measurements by sputtering through a mechanical mask in direct contact with the substrate.

Structural characterization was done by X-ray scattering using a Bruker D8 Discover diffractometer with $\text{Cu } K_\alpha$ radiation and the sample temperature was varied by $\pm 10^\circ\text{C}$ around room temperature by means of a home-built Peltier cooler attached to the sample holder. Measurements of the longitudinal and transverse resistivity were performed in a physical property measurements system (PPMS, Quantum Design). Resistivity measurements were done with a four-point probe on patterned films or in a van der Pauw configuration on planar films. The magnetization was measured in a SQUID magnetometer for magnetic fields up to 5 Tesla applied perpendicular to the film surface.

III. RESULTS AND DISCUSSION

A. Structural characterization

Sputtering without N_2 flow results in the formation of Mn_3Ga with tetragonal structure. Fig. 1(a) shows a symmetrical $\theta/2\theta$ scan of 25 nm Mn_3Ga deposited on MgO (001). The Bragg reflection observed at $2\theta = 51.23^\circ$ corresponds to a lattice plane distance $d = 0.1783$ nm. By comparison with previous studies we assign this peak to the (004) reflection of the tetragonal $D0_{22}$ phase of Mn_3Ga with a lattice constant $c = 0.711 - 0.7133$ nm along the growth direction [26–30]. Mn_3Ga is ferrimagnetic with an easy axis along the crystallographic c axis and a high Curie temperature of 730 K [28, 29].

Supplying a flow $\Phi = 0.6$ sccm N_2 results in a change of the X-ray diffraction diagram with a Bragg peak around 46.91° , see Fig. 1(b) for films deposited on MgO (001) substrates. We identify this peak as the (002) reflection from the cubic Mn_3GaN antiperovskite structure corresponding to a lattice constant $c = 0.3874$ nm along the growth direction in good agreement with bulk Mn_3GaN [31]. The epitaxial growth of the cubic antiperovskite phase is confirmed for $\Phi = 0.6$ sccm by a ϕ -scan of the

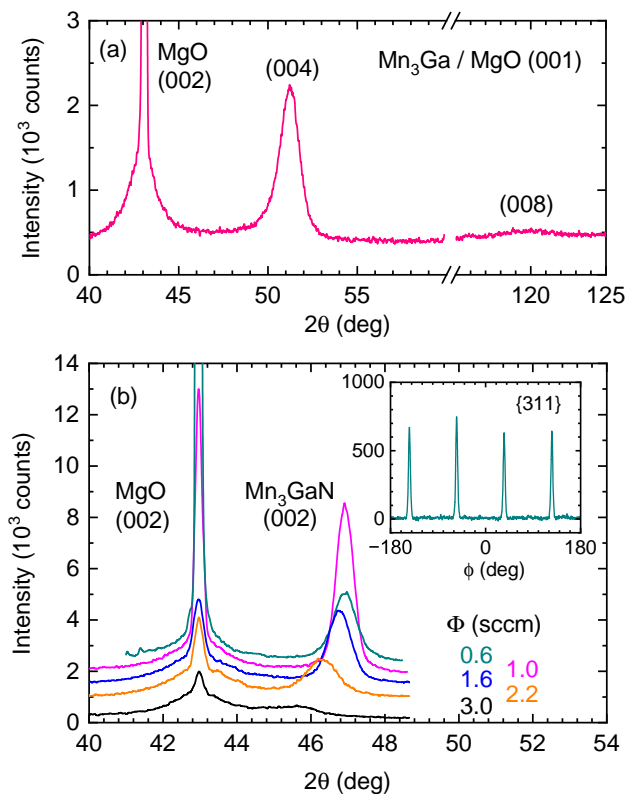


FIG. 1. (a) $\theta/2\theta$ X-ray scan of a 25-nm thick Mn_3Ga film on MgO (001). (b) $\theta/2\theta$ X-ray scans of 25-nm thick Mn_3GaN_x films deposited at different N_2 flows Φ on MgO (001). The sample has been tilted away by $0.5^\circ - 1^\circ$ from the symmetric θ position to reduce the intensity of the strong substrate reflection. Scans have been shifted upward with respect to each other for clarity. Inset shows a ϕ -scan of the {311} planes for the film with $\Phi = 0.6$ sccm confirming the fourfold symmetry of the film and substrate.

{311} planes at $2\theta = 82.55^\circ$ ($d = 0.1172$ nm) around the [001] surface normal, see inset Fig. 1(b). This results in a ratio $c/a = 0.999$ suggesting an almost perfect cubic lattice with negligible tetragonal distortion as reported earlier for a similar low deposition rate of 0.02 nm/s [18]. Due to the large lattice mismatch of 8 % between MgO ($a = 0.4215$ nm) and Mn_3GaN the film is fully relaxed. Increasing the N_2 leads to a shift of the (002) peak to lower scattering angles and to a gradual expansion of the Mn_3GaN lattice.

B. Electronic transport and magnetism

In the following we will focus on the resistivity measurements performed on films prepared under different N_2 gas flows. The temperature dependence of the resistivity ρ , Fig. 2(a), shows a metallic behavior for all films. $\rho(T)$ exhibits a broad and shallow kink around 270 K representing T_N of the antiferromagnetic Γ^{5g} phase [10]. The

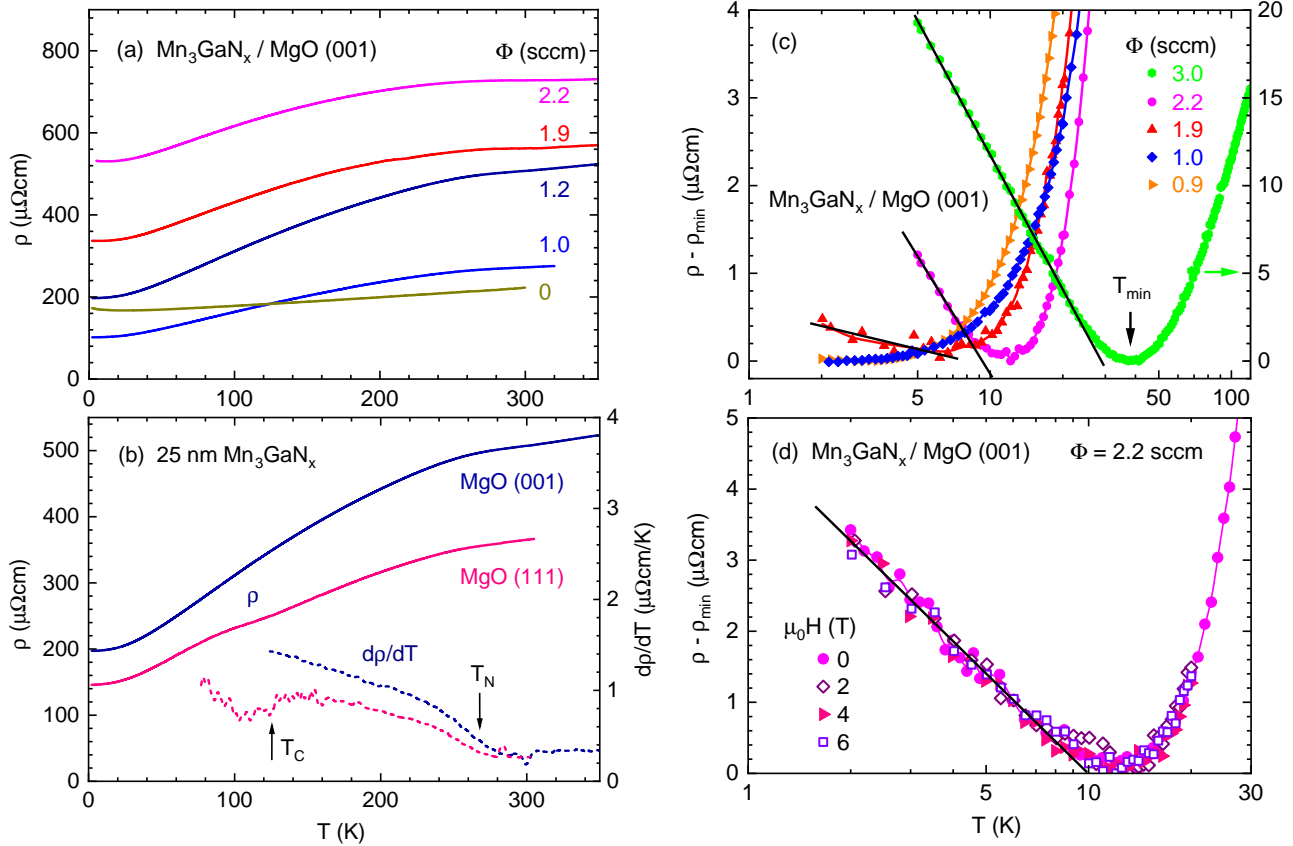


FIG. 2. (a) Resistivity ρ vs temperature T of 25-nm thick Mn_3GaN_x films deposited under different N_2 flows Φ on MgO (100) substrates. (b) $\rho(T)$ of Mn_3GaN_x films on MgO(100) ($\Phi = 1.2$ sccm) and on MgO(111) ($\Phi = 1.0$ sccm). The black solid line indicates a linear behavior to emphasize the broad local maximum of $\rho(T)$ for the film grown on MgO (111). Dashed curves show the derivative $d\rho/dT$ with Curie temperature T_C and Néel temperature T_N indicated by arrows. (c) Semi-logarithmic plot of $\rho - \rho_{\min}$ vs $\log T$ where $\rho_{\min} = \rho(T_{\min})$ indicated by the arrow for the sample prepared under $\Phi = 3.0$ sccm. Solid lines indicate a linear behavior. (d) $\rho - \rho_{\min}$ vs $\log T$ for the film deposited at $\Phi = 2.2$ sccm in different applied magnetic fields H . Solid line indicates a linear behavior.

residual resistivity at low temperatures increases with increasing N_2 gas flow. Note that the film with zero flow represents tetragonal Mn_3Ga with a different structure and should not be compared to the Mn_3GaN_x films. However, a similar metallic-like behavior with a smaller residual resistivity of $30 \mu\Omega\text{cm}$ was reported earlier for 240-nm thick films [30].

Fig. 2(b) shows data of two 25-nm thick films prepared under similar conditions on MgO (001) and (111) substrates. We only mention that Mn_3GaN grows on MgO (111) along the [111] direction with a lattice plane distance $d(111) = 0.2235$ nm corresponding to a lattice constant $c = 0.3871$ nm, similar to the lattice constant for films grown on MgO(001), see above. The broad step in the derivative $d\rho/dT$ corresponding to the kink in $\rho(T)$ indicates a Néel temperature $T_N = 270$ K, a few Kelvin lower than reported for bulk Mn_3GaN [10, 20].

For the film grown on MgO (111), $\rho(T)$ exhibits an additional broad local minimum around 120 K which we attribute to the Curie temperature T_C , see $d\rho/dT$, of a second magnetic phase observed earlier in Mn_3GaN films [22, 23]. Here, the Γ^{5g} phase presumably coexists with a ferrimagnetic-like M-1 phase of tetragonal symmetry and noncollinear and noncoplanar magnetic order [5]. The M-1 phase of Mn_3GaN is particularly interesting because it has been recently suggested as a potential candidate for p-wave magnetic order [32]. Strained films on Pt buffer layers or Mn_3GaN /permalloy heterostructures exhibit enhanced magnetic transition temperatures $T_C = 200$ K and $T_N = 380$ K [23, 33].

Except for the film deposited with $\Phi = 1.0$ sccm, $\rho(T)$ in Fig. 2(c) does not reach a temperature-independent value at low temperatures but instead increases again when cooling to below a temperature T_{\min} , where the

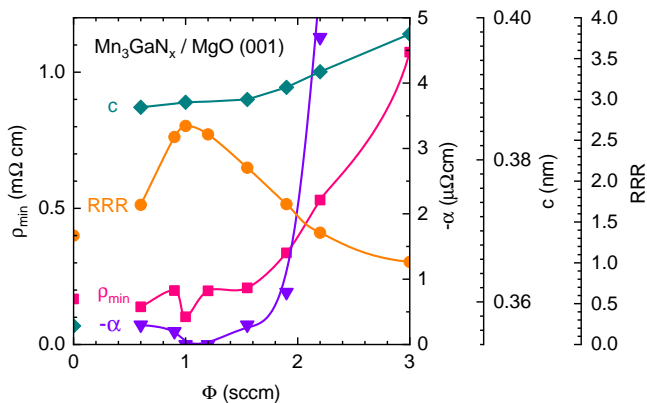


FIG. 3. Characteristic parameters of 25-nm thick Mn₃GaN_x films on MgO (001) substrates vs N₂ flow Φ , see text for details. Solid lines serve as guides to the eye.

minimum resistivity $\rho_{\min} = \rho(T_{\min})$ is considered as the residual resistivity. For $\Phi = 1.0$ sccm (blue squares) we do not observe an increase toward the lowest achievable temperature 1.8 K

The semi-logarithmic plot of $\Delta\rho = \rho(T) - \rho_{\min}$ in Fig. 2(c) clearly shows that $\Delta\rho(T)$ follows a logarithmic temperature dependence $\Delta\rho(T) = \alpha \log(T/T_{\min})$ below T_{\min} with a negative slope $\alpha = d\rho/d\log(T/T_{\min})$. It is important to note that this logarithmic behavior does not depend on the magnetic field applied perpendicular to the sample surface, see Fig. 2(d).

An increase of the resistivity of a metallic film towards lower temperatures could arise from (i) weak localization, (ii) enhanced electron-electron interaction, (iii) Kondo effect, or (iv) scattering of conduction electrons by structural two-level systems. However, quantum interference effects due to weak-localization are known to be very weak in magnetically ordered systems as in the case of Mn₃GaN_x, see below, because of the destructive effect of the exchange field on the phase of the electron wavefunction on time-reversed paths. At low temperatures both types of quantum corrections, weak localization (i) and electron-electron interaction (ii), are expected to change in a magnetic field [34], in contrast to the field-independent resistivity behavior shown in Fig. 2(d). The single-ion magnetic Kondo effect (iii) can hardly occur in a material exhibiting long-range magnetic order where any interaction between magnetic impurities leads to a strong reduction of the Kondo scattering. Moreover, the logarithmic behavior of $\rho(T)$ at low temperatures would be strongly reduced in a magnetic field. Hence, the most important experimental finding is the independence of the logarithmic slope α on an applied magnetic field as large as 6 T suggesting the presence of a nonmagnetic electron scattering mechanism.

A logarithmic behavior of $\rho(T)$ often appears in strongly disordered alloys [35] for which the thermodynamic properties are successfully described by the tunneling model. Here, an atom (or a group of atoms) can tun-

nel between two different states of a double-well potential in configuration space, leading to low-energy excitations that can be modelled as two-level systems (TLS) [36]. The TLS can be considered as an impurity with pseudospin 1/2 coupled to the sea of conduction electrons. This orbital Kondo effect gives rise to a logarithmic $\rho(T)$ dependence around the Kondo temperature T_K [37, 38] and the spin degeneracy of the conduction electron provides two scattering channels [39, 40]. Such a logarithmic temperature dependence of the resistivity attributed to an orbital Kondo effect has been reported for ThAsSe, Ni_xNb_{1-x} metallic glasses, and Mn₅Si₃C_x films [41–43]. This suggests that for the Mn₃GaN_x films the origin of logarithmic increase of $\rho(T)$ toward low temperatures is due to dynamical scatterers, for instance atomic vacancies, displaced or interstitial atoms, or atoms located in grain boundaries. We therefore use the slope α and the temperature T_{\min} as indicators for the amount of structural disorder. The lower the slope and T_{\min} , the higher the structural quality.

The characteristic parameters from X-ray diffraction and electronic transport are summarized in Fig. 3. Films prepared with $\Phi \approx 1$ sccm are characterized by the lowest residual resistance ρ_{\min} , almost zero slope $-\alpha$, and highest residual resistance ratio $RRR = \rho(300\text{ K})/\rho_{\min}$. These films are considered to be grown under optimized conditions.

Next, we discuss the Hall resistivity $\rho_{yx} = \rho_{yx}^A + \rho_{yx}^0$, where ρ_{yx}^A represents the AHE and ρ_{yx}^0 is the ordinary Hall effect arising from the Lorentz force acting on the charge carriers in a perpendicular applied magnetic field. Fig. 4(a,b) shows measurements for films of ferrimagnetic Mn₃Ga and antiperovskite Mn₃GaN_x prepared under optimized growth conditions.

For the ferrimagnetic Mn₃Ga film [Fig. 4(a)], we observe a broad hysteresis of ρ_{yx} with a coercivity $\mu_0 H_c \approx 2$ T that barely shrinks when comparing data at 50 K and 300 K due to the high $T_C = 730$ K [28, 29]. From ρ_{yx} we have subtracted the linear-in-field contribution $\rho_{yx}^0 = R_H \mu_0 H$. From a plot of $\rho_{yx} - R_H \mu_0 H$ vs H we varied R_H until a field-independent AHE was achieved at magnetic saturation with $R_H = 10^{-3} \text{ cm}^3/\text{As}$. The obtained value $\rho_{yx}^A = 1.8 \mu\Omega\text{cm}$ at 300 K corresponds to a Hall conductivity $\sigma_{xy}^A \approx \rho_A/\rho^2 = 36.5 \Omega^{-1}\text{cm}^{-1}$ for tetragonal Mn₃Ga. Very similar values for the coercivity and Hall resistivity have been previously reported for 240-nm thick films on Mg (001) substrates [30].

For an antiperovskite Mn₃GaN_x film [Fig. 4 (b)] no AHE is observed for $T > 120$ K and only the ordinary Hall effect linear in field appears. This is in line with the fact that for a cubic and structurally relaxed antiperovskite Mn₃GaN with Γ^{5g} magnetic structure no AHE is expected [14, 15]. However, below $T_C \approx 120$ K where a phase of coexisting Γ^{5g} and M-1 magnetic order presumably exists, an AHE is observed. By the same method as mentioned above we obtain $\rho_{yx}^A = 0.036 \mu\Omega\text{cm}$, $R_H = 0.9 \times 10^{-4} \text{ cm}^3/\text{As}$, and $\sigma_{xy}^A = 3.0 \Omega^{-1}\text{cm}^{-1}$ for the 50-nm thick film at 50 K. R_H is a factor of two smaller

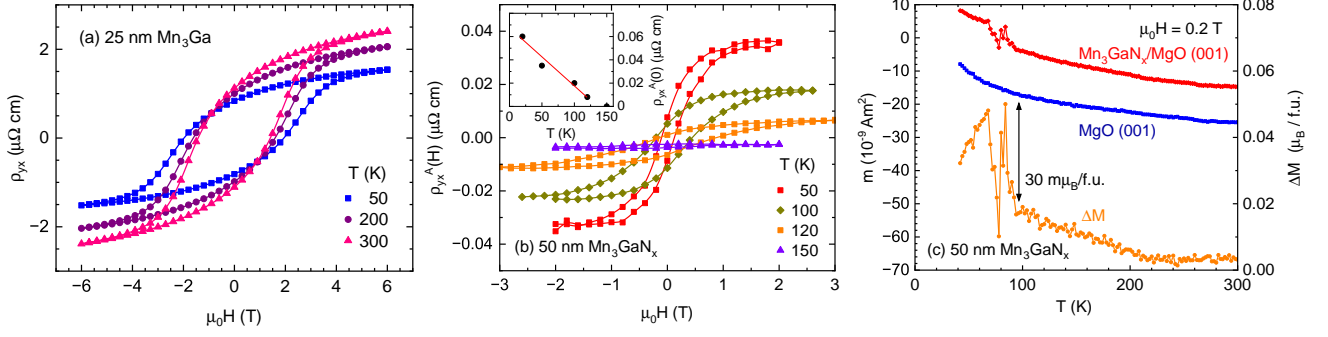


FIG. 4. Hall resistivity ρ_{yx} vs applied magnetic field H at different temperatures T for (a) a Mn_3Ga film and (b) a Mn_3GaN_x film ($\Phi = 1.0 \text{ sccm}$) deposited on MgO (001) substrates. Inset shows the AHE at zero field vs temperature. (c) Magnetic moment of the Mn_3GaN_x film on MgO (001) (red) and of the bare MgO substrate (blue). Orange data show the magnetization ΔM of the Mn_3GaN_x film obtained after subtraction of the substrate data (blue) and a paramagnetic background from the raw data (red).

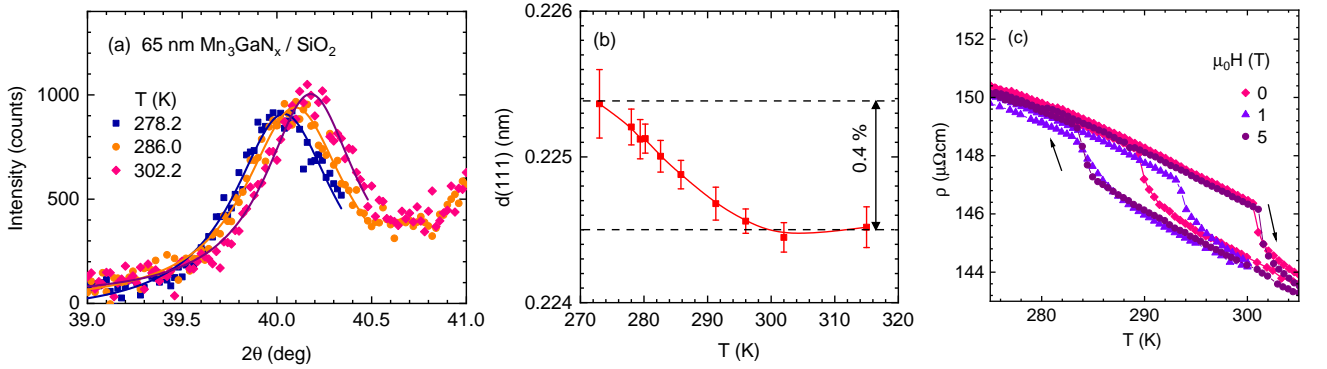


FIG. 5. (a) $\theta/2\theta$ X-ray scans of a 65-nm thick Mn_3GaN_x film on SiO_2 at different ambient temperatures T . (b) Lattice parameter d determined from the (111) Bragg reflection. (c) Resistivity $\rho(T)$ around the phase transition for different applied magnetic fields H .

than $R_H = 2 \times 10^{-4} \text{ cm}^3/\text{As}$ [23] obtained for strained Mn_3GaN films, possibly due to a smaller fraction of the ferrimagnetic-like M-1 phase.

The two magnetic phases of Mn_3GaN_x film are also observed in magnetization measurements. Since the magnetization of the thin film is very small, the SQUID magnetometer records strong fluctuations of the signal as soon as the magnetic moment m of the sample vanishes, see raw data (red) around $m \approx 0$ in Fig. 4(c). Therefore, we measured m of the bare substrate (blue) and subtracted these data and a paramagnetic background from the raw data. The observed magnetization ΔM of Mn_3GaN_x , Fig. 4(c) (orange) shows a continuous increase up to $20 \text{ m}\mu_B/\text{f.u.}$ when cooling down in the Γ^{5g} phase below T_N and a sudden jump around 100 K of $\Delta M = 30 \text{ m}\mu_B/\text{f.u.}$ corresponding to $0.01 \mu_B/\text{Mn}$ which we attribute to the ferrimagnetic-like phase below T_C . This latter value is smaller than $0.2 \mu_B/\text{Mn}$ and $0.08 \mu_B/\text{Mn}$ previously reported in bulk and thin film Mn_3GaN , respectively, supporting our claim that the fraction of the M-1 phase in the present film is smaller [5, 23].

C. Lattice distortion at T_N

Mn_3GaN is known to exhibit a distortion of the cubic lattice by 0.4 % when the temperature changes across T_N [20, 31, 33]. For resolving this lattice distortion in the Mn_3GaN_x films by X-ray diffraction we have grown thicker films on glass substrates in order to avoid reflections from the single-crystalline MgO substrate. Fig. 5(a) shows that with increasing temperature the (111) Bragg reflection of Mn_3GaN (strongest line) shifts to higher diffraction angles corresponding to a decrease of the lattice parameter $d(111)$ along the surface normal. From the temperature dependence of $d(111)$ shown in Fig. 5(b) a strong compression of 0.4 % of the lattice along the surface normal is observed in a temperature interval of $\pm 15 \text{ K}$ around 285 K . Note that this temperature dependence is opposite to what is expected from the usually observed thermal expansion for solid materials. We mention that similar results have been obtained for Mn_3GaN_x films deposited under optimized conditions on other substrates like Si (100) and diamond. In each

case we observe a compression of the Mn_3GaN lattice along the surface normal. We attribute this to the transition from the antiferromagnetic to the paramagnetic phase above across T_N and the strong coupling between the crystalline lattice and the magnetic order.

The structural phase transition accompanied with the magnetic phase transition is also observed in the $\rho(T)$ behavior of these films, Fig. 5(c), with a broad hysteresis of similar magnitude. We do not observe a clear dependence on the applied magnetic field except that the transition takes place at different temperatures in subsequent thermal cycles possibly due to supercooling/superheating effects in a regime of metastable states.

IV. CONCLUSION

Mn_3GaN_x films of antiperovskite structure were grown by reactive dc magnetron sputtering. The detailed study of the resistivity of films prepared under different N_2

gas fluxes Φ shows that the sputtering conditions can be optimised to obtain films with the required magnetic and structural phase transitions by relying on parameters such as resistivity, the ratio of the residual resistivity and, in particular, a vanishing increase in resistivity at low temperatures. In the present case, a N_2 flow $\Phi \approx 1$ sccm has been found to be beneficial for obtaining Mn_3GaN_x films with minimized structural disorder. We propose that this path can be followed in search for optimal conditions for growing of other antiperovskite nitrides.

ACKNOWLEDGEMENTS

This work was supported by the Sino-German Mobility Programme No. M-0273.

-
- [1] Y. Wang, H. Zhang, J. Zhu, X. Lü, S. Li, R. Zou, and Y. Zhao, Antiperovskites with Exceptional Functionalities, *Advanced Materials* **32**, 1905007 (2020).
- [2] J. M. D. Coey, D. Givord, and D. Fruchart, Metallic Nitride and Carbide Perovskites: History and Prospects, *ECS J. Solid State Sci. Technol.* **11**, 055002 (2022).
- [3] H. K. Singh, I. Samathrakas, N. M. Fortunato, J. Zemen, C. Shen, O. Gutfleisch, and H. Zhang, Multifunctional antiperovskites driven by strong magnetostructural coupling, *npj Comput Mater* **7**, 1 (2021).
- [4] K. Takenaka, M. Ichigo, T. Hamada, A. Ozawa, T. Shibayama, T. Inagaki, and K. Asano, Magnetovolume effects in manganese nitrides with antiperovskite structure, *Science and Technology of Advanced Materials* **15**, 015009 (2014).
- [5] K. Shi, Y. Sun, J. Yan, S. Deng, L. Wang, H. Wu, P. Hu, H. Lu, M. I. Malik, Q. Huang, and C. Wang, Baromagnetic Effect in Antiperovskite $\text{Mn}_3\text{Ga}_{0.95}\text{N}_{0.94}$ by Neutron Powder Diffraction Analysis, *Advanced Materials* **28**, 3761 (2016).
- [6] J. Zemen, Z. Gercsi, and K. G. Sandeman, Piezomagnetism as a counterpart of the magnetovolume effect in magnetically frustrated Mn-based antiperovskite nitrides, *Phys. Rev. B* **96**, 024451 (2017).
- [7] P. Lukashev, R. F. Sabirianov, and K. Belashchenko, Theory of the piezomagnetic effect in Mn-based antiperovskites, *Phys. Rev. B* **78**, 184414 (2008).
- [8] M. Mochizuki, M. Kobayashi, R. Okabe, and D. Yamamoto, Spin model for nontrivial types of magnetic order in inverse-perovskite antiferromagnets, *Phys. Rev. B* **97**, 060401 (2018).
- [9] O. Gomonay, Berry-phase effects and electronic dynamics in a noncollinear antiferromagnetic texture, *Phys. Rev. B* **91**, 144421 (2015).
- [10] D. Fruchart and E. F. Bertaut, Magnetic Studies of the Metallic Perovskite-Type Compounds of Manganese, *J. Phys. Soc. Jpn.* **44**, 781 (1978).
- [11] H. Chen, L. Liu, X. Zhou, Z. Meng, X. Wang, Z. Duan, G. Zhao, H. Yan, P. Qin, and Z. Liu, Emerging Antiferromagnets for Spintronics, *Advanced Materials* **36**, 2310379.
- [12] V. Baltz, A. Manchon, M. Tsoi, T. Moriyama, T. Ono, and Y. Tserkovnyak, Antiferromagnetic spintronics, *Rev. Mod. Phys.* **90**, 015005 (2018).
- [13] T. Jungwirth, X. Marti, P. Wadley, and J. Wunderlich, Antiferromagnetic spintronics, *Nature Nanotech* **11**, 231 (2016).
- [14] G. Gurung, D.-F. Shao, T. R. Paudel, and E. Y. Tsymlal, Anomalous Hall conductivity of noncollinear magnetic antiperovskites, *Phys. Rev. Mater.* **3**, 044409 (2019).
- [15] I. Samathrakas and H. Zhang, *Phys. Rev. B* **101**, 214423 (2020).
- [16] K. Takenaka, T. Sugiura, Y. Kadowaki, M. Ozeki, Y. Okamoto, and A. Fujita, Giant Magneto-Volume and Magneto-Caloric Effects of Frustrated Antiferromagnet Mn_3GaN under Hydrostatic Pressure, *J. Phys. Soc. Jpn.* **90**, 044601 (2021).
- [17] W. J. Feng, D. Li, Y. F. Deng, Q. Zhang, H. H. Zhang, and Z. D. Zhang, *J Mater Sci* **45**, 2770 (2010).
- [18] S. Ishino, J. So, H. Goto, T. Hajiri, and H. Asano, Preparation and evaluation of $\text{Mn}_3\text{Ga}_{1-x}\text{N}_x$ thin films with controlled N compositions, *AIP Advances* **8**, 056312 (2017).
- [19] H. Han, Y. Sun, K. Shi, X. Yuan, J. Ren, J. Cui, D. Hu, K. Zhang, and C. Wang, Sign reversal of the anomalous Hall effect in antiperovskite (110)-oriented $\text{Mn}_{3.19}\text{Ga}_{0.81}\text{N}_{1-\delta}$ film, *Journal of Applied Physics* **132**, 233902 (2022).
- [20] D. Kasugai, A. Ozawa, T. Inagaki, and K. Takenaka, Effects of nitrogen deficiency on the magnetostructural properties of antiperovskite manganese nitrides, *Journal of Applied Physics* **111**, 07E314 (2012).
- [21] B. H. Rimmler, B. K. Hazra, B. Pal, K. Mohseni, J. M. Taylor, A. Bedoya-Pinto, H. Deniz, M. Tangi, I. Kostanovskiy, C. Luo, R. R. Neumann, A. Ernst,

- F. Radu, I. Mertig, H. L. Meyerheim, and S. S. P. Parkin, Atomic Displacements Enabling the Observation of the Anomalous Hall Effect in a Non-Collinear Antiferromagnet, *Advanced Materials* **35**, 2209616 (2023).
- [22] T. Hajiri, S. Ishino, K. Matsuura, and H. Asano, Electrical current switching of the noncollinear antiferromagnet Mn₃GaN, *Applied Physics Letters* **115**, 052403 (2019).
- [23] T. Hajiri, K. Matsuura, K. Sonoda, E. Tanaka, K. Ueda, and H. Asano, Spin-Orbit-Torque Switching of Non-collinear Antiferromagnetic Antiperovskite Manganese Nitride, *Phys. Rev. Appl.* **16**, 024003 (2021).
- [24] J. T. Gudmundsson, Physics and technology of magnetron sputtering discharges, *Plasma Sources Sci. Technol.* **29**, 113001 (2020).
- [25] N. F. Azevedo Neto, D. M. G. Leite, P. N. Lisboa-Filho, and J. H. D. da Silva, Role of the reactive sputtering deposition power in the phase control of cobalt oxide films, *Journal of Vacuum Science & Technology A* **36**, 061512 (2018).
- [26] E. Krén and G. Kádár, Neutron diffraction study of Mn₃Ga, *Solid State Communications* **8**, 1653 (1970).
- [27] H. Niida, T. Hori, and Y. Nakagawa, Magnetic Properties and Crystal Distortion of Hexagonal Mn₃Ga, *J. Phys. Soc. Jpn.* **52**, 1512 (1983).
- [28] B. Balke, G. H. Fecher, J. Winterlik, and C. Felser, Mn₃Ga, a compensated ferrimagnet with high Curie temperature and low magnetic moment for spin torque transfer applications, *Applied Physics Letters* **90**, 152504 (2007).
- [29] H. Kurt, K. Rode, M. Venkatesan, P. Stamenov, and J. M. D. Coey, High spin polarization in epitaxial films of ferrimagnetic Mn₃Ga, *Phys. Rev. B* **83**, 020405 (2011).
- [30] H.-W. Bang, W. Yoo, C. Kim, S. Lee, J. Gu, Y. Park, K. Lee, and M.-H. Jung, Structural, magnetic, and electrical properties of collinear antiferromagnetic heteroepitaxy cubic Mn₃Ga thin films, *Applied Physics Letters* **115**, 012402 (2019).
- [31] K. Takenaka, T. Inagaki, and H. Takagi, Conversion of magnetic structure by slight dopants in geometrically frustrated antiperovskite Mn₃GaN, *Applied Physics Letters* **95**, 132508 (2009).
- [32] A. B. Hellenes, T. Jungwirth, J. Sinova, and L. Šmejkal, Unconventional p-wave magnets (2023), arXiv:2309.01607.
- [33] T. Nan, C. X. Quintela, J. Irwin, G. Gurung, D. F. Shao, J. Gibbons, N. Campbell, K. Song, S.-Y. Choi, L. Guo, R. D. Johnson, P. Manuel, R. V. Chopdekar, I. Hallsteinsen, T. Tybell, P. J. Ryan, J.-W. Kim, Y. Choi, P. G. Radaelli, D. C. Ralph, E. Y. Tsymbal, M. S. Rzchowski, and C. B. Eom, Controlling spin current polarization through non-collinear antiferromagnetism, *Nat Commun* **11**, 4671 (2020).
- [34] P. A. Lee and T. V. Ramakrishnan, Disordered electronic systems, *Rev. Mod. Phys.* **57**, 287 (1985).
- [35] R. W. Cochrane, R. Harris, J. O. Ström-Olson, and M. J. Zuckermann, Structural Manifestations in Amorphous Alloys: Resistance Minima, *Phys. Rev. Lett.* **35**, 676 (1975).
- [36] W. A. Phillips (Editor), *Amorphous Solids* (Springer, Berlin, 1981).
- [37] A. Zawadowski, Kondo-like State in a Simple Model for Metallic Glasses, *Phys. Rev. Lett.* **45**, 211 (1980).
- [38] K. Vladár and A. Zawadowski, Theory of the interaction between electrons and the two-level system in amorphous metals. III. Experimentally observable quantities, *Phys. Rev. B* **28**, 1596 (1983).
- [39] D. L. Cox and A. Zawadowski, Exotic Kondo effects in metals: Magnetic ions in a crystalline electric field and tunnelling centres, *Advances in Physics* **47**, 599 (1998).
- [40] J. von Delft, D. C. Ralph, R. A. Buhrman, S. K. Upadhyay, R. N. Louie, A. W. W. Ludwig, and V. Ambegaokar, The 2-Channel Kondo Model: I. Review of Experimental Evidence for Its Realization in Metal Nanoconstrictions, *Annals of Physics* **263**, 1 (1998).
- [41] T. Cichorek, A. Sanchez, P. Gegenwart, F. Weickert, A. Wojakowski, Z. Henkie, G. Auffermann, S. Paschen, R. Kniep, and F. Steglich, Two-Channel Kondo Effect in Glasslike ThAsSe, *Phys. Rev. Lett.* **94**, 236603 (2005).
- [42] A. Halbritter, O. Y. Kolesnychenko, G. Mihály, O. I. Shklyarevskii, and H. van Kempen, Transport properties and point-contact spectra of NixNb_{1-x} metallic glasses, *Phys. Rev. B* **61**, 5846 (2000).
- [43] B. Gopalakrishnan, C. Sürgers, R. Montbrun, A. Singh, M. Uhlarz, and H. v. Löhneysen, Electronic transport in magnetically ordered Mn₅Si₃ films, *Phys. Rev. B* **77**, 104414 (2008).